



# Microstructure and mechanical properties of ADC12 composites reinforced with graphene nanoplates prepared by ultrasonic assisted casting

Jun-jie XIONG<sup>1,2</sup>, Hong YAN<sup>1,2</sup>

1. School of Mechanical and Electrical Engineering, Nanchang University, Nanchang 330031, China;
2. Key Laboratory of Light Alloy Preparation and Processing in Nanchang City, Nanchang 330031, China

Received 15 January 2020; accepted 4 September 2020

**Abstract:** Microstructure and mechanical properties of ADC12 composites reinforced with graphene nanoplates (GNPs) prepared by high-intensity ultrasonic assisted casting were investigated. The results indicated that high-intensity ultrasound can promote the uniform distribution of GNPs in the melt, resulting in refining the  $\alpha(\text{Al})$  phase and Si phase. The optimal addition of GNPs was 0.9 wt.%, and the optimal ultrasonic time was 12 min. The tensile strength, the yield strength and the hardness of the composite produced under the optimal parameters were 256.8 MPa, 210.6 MPa and HV 126.0, respectively, which increased by 30.5%, 42.7%, and 34.8% compared with those of the matrix, respectively. After adding the GNPs, the fracture mechanism gradually turned from a brittle fracture to a ductile fracture. The good interface and distribution allowed GNPs to play the role in fine grain strengthening, dislocation strengthening and load transfer strengthening effectively.

**Key words:** ADC12 composite; graphene nanoplate (GNP); casting; microstructure; mechanical properties

## 1 Introduction

With the development of society, new energy vehicles have become the mainstream of the automotive industry. In order to achieve lightweight, most new energy automobile parts are manufactured by using aluminum alloys [1]. However, pure aluminum alloys sometimes do not meet the performance requirements fully. At this time, aluminum matrix composites with good performance can come in handy [2–4]. As an important member of the nano-carbon material family, graphene has excellent mechanical, electrical and thermal properties, which is considered to be the most attractive nano-reinforced phase for the development of high-performance metal matrix composites [5–7].

For improving the comprehensive mechanical properties of aluminum alloys, adding the graphene or graphene ceramic binary powders to the aluminum matrix has become a research hotspot in the field of aluminum metal composites [8–10]. LIU et al [11] prepared 6061Al aluminum matrix composites reinforced with Ni-coated graphene nanoplates (GNPs) by ball milling and hot-pressing sintering. Studies revealed that the yield strength and tensile strength of the composite with 0.7 wt.% GNPs addition reached 140 and 213 MPa, respectively, which were 75% and 30% higher than those of the matrix alloy, respectively. BHADAURIA et al [12] prepared Al–GNPs composites by discharge plasma sintering. As a result, the yield strength of the composites with 0.5 wt.% GNPs increased by 98% compared with that of the matrix. An agglomeration appeared in

**Foundation item:** Project (51965040) supported by the National Natural Science Foundation of China; Project (20181BAB206026) supported by the Natural Science Foundation of Jiangxi Province, China

**Corresponding author:** Hong YAN; Tel: +86-791-83969622; E-mail: [hyan@ncu.edu.cn](mailto:hyan@ncu.edu.cn)

DOI: 10.1016/S1003-6326(20)65455-3

the aluminum matrix when GNP content was increased to 1.0 wt.%. LI et al [13] achieved Al–GNP aluminum matrix composites by continuous casting and rolling techniques. The tensile strength of Al–0.2wt.% GNPs was 36.8% higher than that of pure Al matrix prepared under the same conditions, resulting from the layered structure of GNPs and the effects of load transfer. ZENG et al [14] prepared graphene-reinforced aluminum matrix composites via solution mixing and powder metallurgy. As a result, a tensile strength of 255 MPa was achieved for the graphene/Al composites with 0.3 wt.% graphene, which had a 25% increase over the tensile strength of the pure Al matrix.

Currently, powder metallurgy and casting processes were mainly used to prepare graphene-reinforced aluminum metal composites. For the powder metallurgy process [15,16], it was not suitable for large-scale industrial production because of its high cost and difficult processing. However, the casting process had a low preparation cost, simple operation steps and equipment requirements, making it easier to adapt to modern industrial production [17,18]. AYDIN et al [19] studied different casting methods such as lost foam casting, sand casting, die casting, ceramic mold casting and squeeze casting. They found that the incorporation of the graphene was established by only squeeze casting method. The produced samples were subjected to bending tests, and it was found that 25% increase in bending strength was achieved by 0.1 wt.% graphene to the matrix alloy. VENKATESAN and XAVIOR [20] also fabricated metal matrix composites based on AA7050 alloy reinforced with graphene nanoparticles by stir casting and squeeze casting techniques. However, increasing the graphene content beyond 0.3 wt.% resulted in cluster formation. Hence, there was a limitation adding a high content of GNPs to the matrix alloy by the squeeze casting. Compared with other casting methods, the ultrasonic assisted casting can increase the content of reinforcing phases in the matrix, and ultrasound dispersion was an efficient method to obtain finely dispersed particles in the melt. In addition, studies have shown that the introduction of high-intensity ultrasonic waves into the melt could achieve good results in the preparation of metal matrix composite

materials [21,22]. Besides, the research of the casting combined with ultrasound on the graphene-reinforced metal matrix composites has been still in its infancy, so it will be a good choice to prepare aluminum matrix composites reinforced with graphene by high-intensity ultrasonic casting.

As a near-eutectic Al–Si–Cu alloy [23–25], ADC12 aluminum alloy was widely used in the automotive industry such as the manufacture of automobile cylinders, boxes, frames and pistons due to the good properties including low density, high specific strength, good fluidity and low thermal expansion coefficient. However, some coarse phases of the structure in the ADC12 alloy by the casting process have caused the reduction of its mechanical properties. In combination with the high-performance advantages of graphene, the using of graphene as the reinforcement of the ADC12 alloy will expand its a wider application value, which has a great research potential.

In this work, Al–GNPs intermediate prefabricated block was prepared by powder metallurgy, and the small intermediate preform was added to the ADC12 alloy melt by high-intensity ultrasonic casting method for preparing ADC12–GNPs aluminum metal composites. The effects of different ultrasonic processes on the microstructure and mechanical properties of the composites were studied. The strengthening mechanism was discussed. This provided a reference for the development and application of graphene in the field of aluminum metal composites.

## 2 Experimental

### 2.1 Original materials

The matrix material is Al–Si–Cu series of aluminum alloy, and its grade is ADC12. The chemical composition is listed in Table 1.

**Table 1** Chemical composition of ADC12 alloy (wt.%)

Si	Cu	Mg	Zn	Fe	Mn	Al
10.13	3.02	0.26	0.58	0.55	0.33	Bal.

The aluminum powder used in the experiment is high-purity (purity  $\geq 99\%$ ). From the SEM image shown in Fig. 1(a), the shape of Al particles is nearly spherical. The average particle size is about 128  $\mu\text{m}$ , as shown in Fig. 1(b).

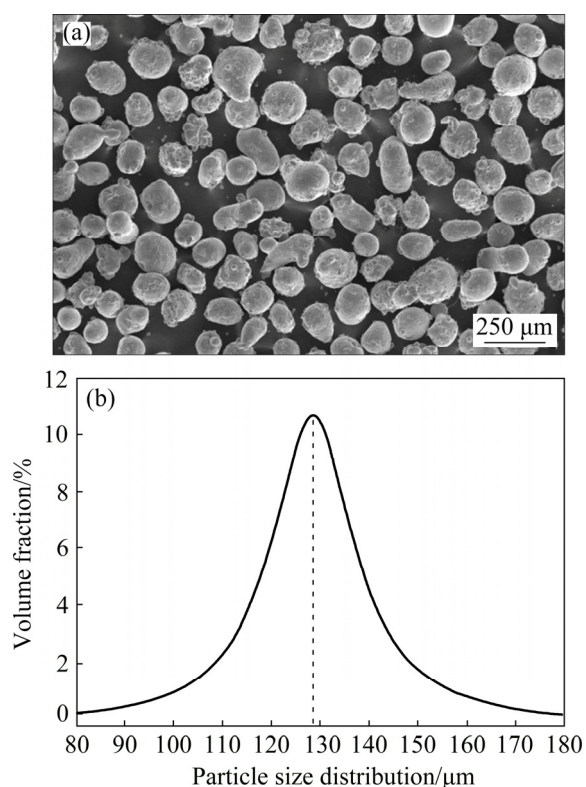


**Fig. 1** Al powders used in present work: (a) SEM microstructure; (b) Particle size distribution

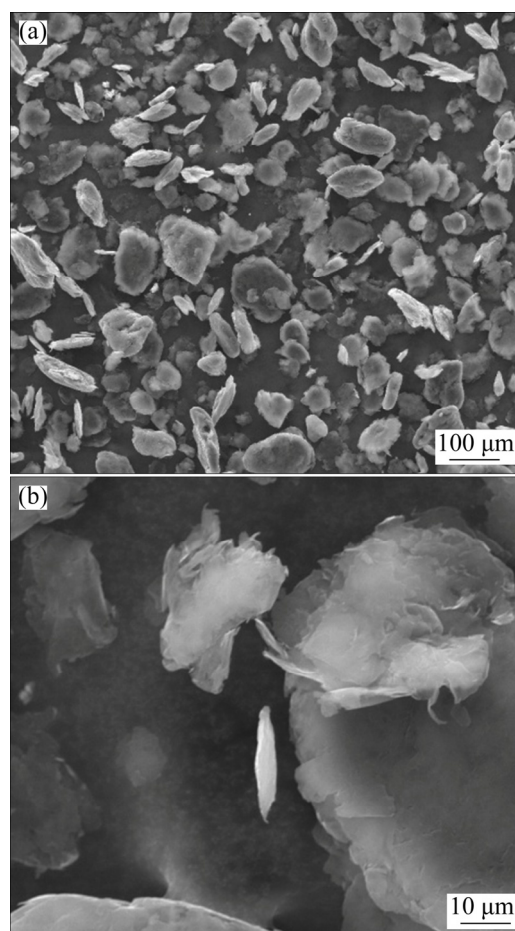
The GNPs are produced by Chengdu Organic Chemistry Co., Ltd., Chinese Academy of Sciences. The GNPs prepared by the company have the average thickness of 5 nm, the average micro-sheet size of 6  $\mu\text{m}$ , and the average amount of 15 layers. The SEM morphology is shown in Fig. 2. It can be seen that the graphene nanosheets have a wrinkled sheet-like morphology from Fig. 2(a). It is easy to agglomerate due to the high specific surface energy and specific surface area of GNPs. A small number of graphene nanosheets with small size and few layers can be seen in the high magnification morphology, as shown in Fig. 2(b).

Figure 3 shows the XRD pattern of graphene nanoplates. It can be seen that there are a strong diffraction peak at the  $2\theta$  angle of  $26.38^\circ$  and a clear diffraction peak at the  $2\theta$  angle of  $54.54^\circ$ , and the corresponding crystal plane indexes are (002) and (004), respectively, which can be determined as the diffraction peaks of graphene by the diffraction cards [26].

## 2.2 Prepared materials

### 2.2.1 Preparation of Al–GNPs prefabricated block

The GNPs were added in the form of



**Fig. 2** SEM morphology of graphene nanoplates: (a) Low magnification; (b) High magnification

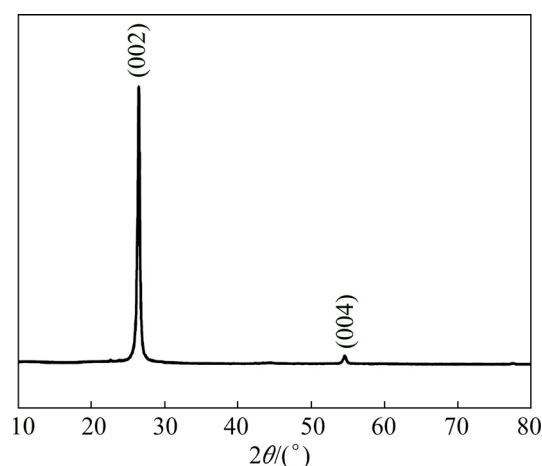


**Fig. 3** XRD pattern of graphene nanoplates

prefabricated block. GNPs were blended in a proportion of 6 wt.% of the mixed powders (aluminum powder and graphene nanosheets). The specific steps were as follows. Firstly, GNPs were added into pure ethanol and dispersed with an ultrasonic cleaner for about 100 min (the ultrasonic power was 480 W, and the frequency was 40 kHz).

Secondly, aluminum powder and absolute ethanol were mixed in a beaker by mechanical stirring, the stirring speed was 100 r/min, and the time was 100 min. Then, the aluminum powder was uniformly sprinkled into the ultrasonic alcohol and GNPs solution, and the time of the ultrasonic and stirring was 60 min again (keeping the same process parameters). After completing the ultrasonic and stirring, the mixed powder alcohol suspension was placed under the magnetic stirrer for magnetic stirring. The heating temperature was 50 °C, and the stirring speed was 1500 r/min. Thirdly, the mixed powders were dried at 323 K under vacuum for 24 h. Then, the dried mixed powders were pressed into a mold under 60 MPa. After shaping, the powders were sintered under vacuum in the sintering furnace at the sintering temperature of 400 °C and the sintering time of 60 min. Finally, the Al–GNPs intermediate prefabricated block was obtained. The block was cut into some small particles for using.

### 2.2.2 Preparation of ADC12–GNPs composite

Firstly, the graphite crucible was dried, and the casting mold was preheated to 200 °C in a heat treatment furnace. The ADC12 alloy was cut into small pieces for using. The prepared Al–GNPs intermediate block particles were covered with the aluminum foil. Secondly, the weighed ADC12 alloy was put into the graphite crucible, then placing the crucible in the resistance furnace for heating to

780 °C, followed by holding for 20 min. Thirdly, the small Al–GNPs intermediate particles were added to the melt in batches at different angles. The total mass of the intermediate preform added to the melt was calculated according to the mass fraction (0, 0.3, 0.6, 0.9, 1.2 wt.%) of GNPs in the melt. At the same time, high-intensity ultrasound was applied while GNPs were added. The ultrasonic power was 2.8 kW, ultrasonic frequency was 20 kHz, and ultrasound time was 12 min. The melt was poured into the preheated mold after the ultrasound. In order to study the effects of ultrasonic time on the microstructure of the composite, the ultrasonic power and frequency remained unchanged, the ultrasonic time of 6, 12, and 18 min was adopted to prepare the ADC12–0.9GNPs composite, respectively. Argon was filled to protect the melt during the entire experiment. The flow chart is shown in Fig. 4.

### 2.3 Performance testing and material characterization

The microstructure of the alloy sample was observed by an optical microscope (Nikon ECLIPSE MA200) and a scanning electron microscope (SEM, VEGA3) equipped with an energy diffraction spectrometer. The sample was etched by 0.5% HF solution. The grain size was measured by Image-Pro Plus software. The D8SOCur diffractometer was used for X-ray

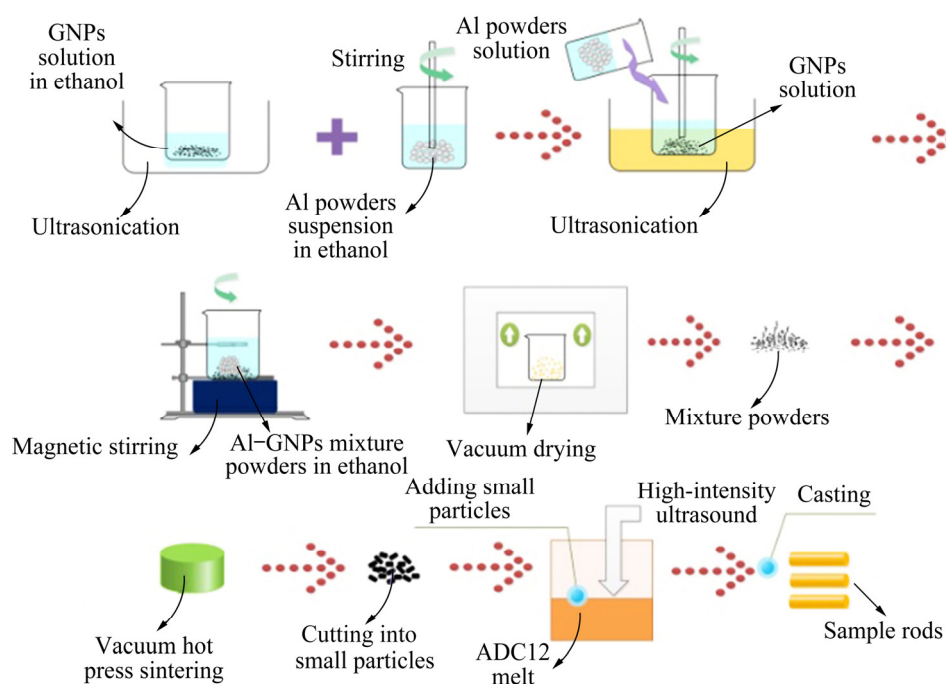


Fig. 4 Schematic diagram of material processing

diffraction analysis of the material. Raman measurement was performed by JY-HR800 laser Raman spectrometer. The hardness of the material was measured by a HVS-1000A hardness instrument, applying a load of 200 g with a load time of 15 s. The tensile test was carried out at a rate of 1 mm/min by UTM5105 tension machine. The test samples were machined into tensile test bars with a diameter of 10 mm and a gauge length of 50 mm. The transmission electron microscope (TEM, JEM-2100) was used to characterize the micro-interface structure between GNPs and the matrix.

### 3 Results and discussion

#### 3.1 Raman spectroscopy

Figure 5 shows the Raman spectra of GNPs. It can be concluded that the abscissa values corresponding to the D and G peaks are 1350 and 1580  $\text{cm}^{-1}$ , respectively. The smaller the ratio of the integrated intensity of the D peak to G peak (i.e.,  $I_D/I_G$ ), the more the integral the graphene

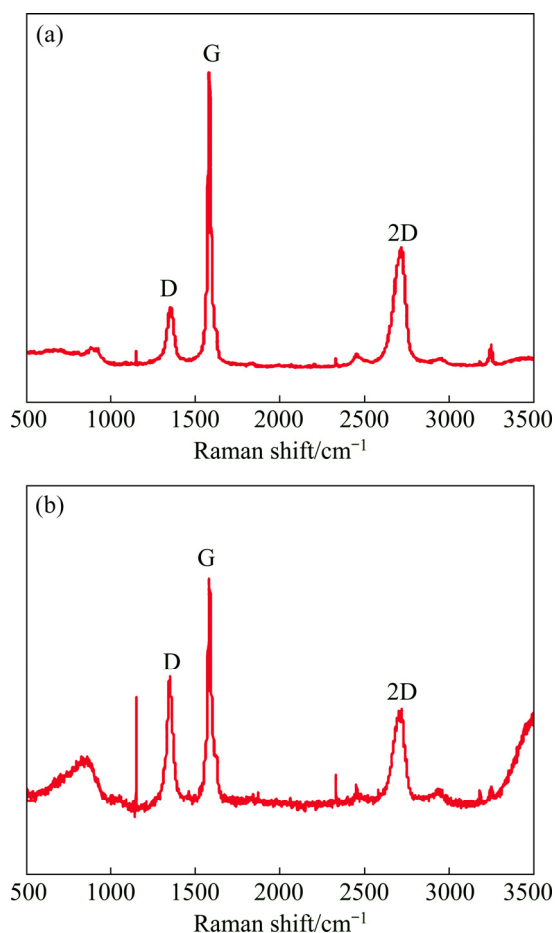


Fig. 5 Raman spectra of raw GNPs (a) and Al-GNPs (b)

structure [27,28]. The  $I_D/I_G$  value of the original GNPs is 0.19, which is relatively small. Therefore, the structure of the used GNPs is relatively integral, as shown in Fig. 5(a). Figure 5(b) shows the Raman spectrum of mixed Al-GNPs powders. The integrated intensity ratio of the D peak to the G peak is 0.72, which is a small value. Therefore, compared with the original GNPs, the structural integrity of GNPs in the mixed powders has not been destroyed.

#### 3.2 Microstructures of ADC12-GNPs composites

##### 3.2.1 XRD comparison

Figure 6 shows the XRD patterns of the matrix and composites with different GNPs additions. It can be seen that there are diffraction peaks of Al, Si and  $\text{CuAl}_2$  phases in the matrix alloy. There is no peak at the position of spectrum C(002) when the content of GNPs added is 0.3 wt.% or 0.6 wt.%. X-ray diffractometer is difficult to be detected due to the low content of GNPs. A weak C(002) characteristic peak can be observed at the position where  $2\theta$  is  $26.38^\circ$  when the content of GNPs is 0.9 wt.%. A more prominent C(002) characteristic peak is observed at this position when the content of GNPs is 1.2 wt.%.

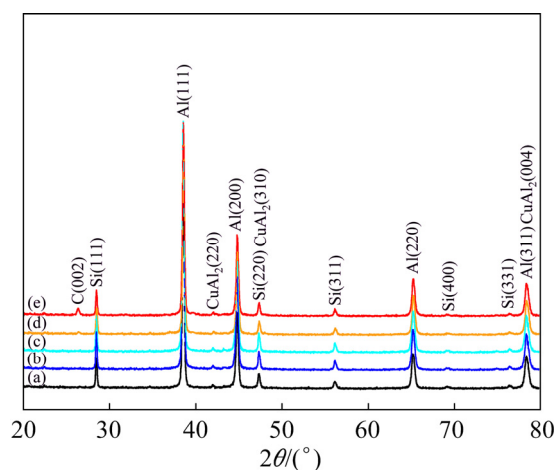


Fig. 6 XRD patterns of ADC12 alloy composite with different contents of GNPs: (a) ADC12; (b) ADC12-0.3GNPs; (c) ADC12-0.6GNPs; (d) ADC12-0.9GNPs; (e) ADC12-1.2GNPs

##### 3.2.2 Microstructures of ADC12-GNPs composites with different graphene additions

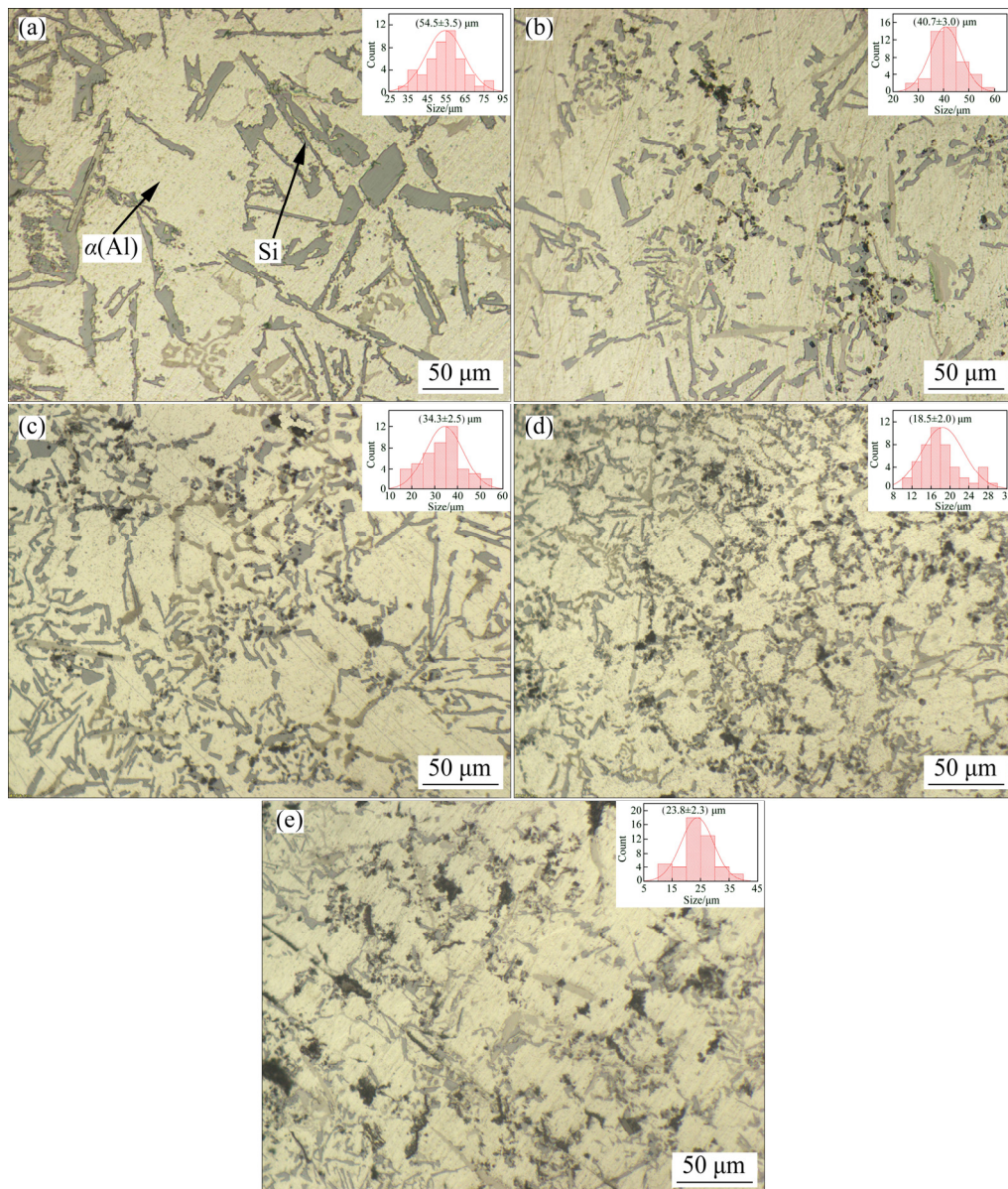
The microstructures of the matrix and composites with different graphene additions prepared under the same conditions are shown in

Fig. 7. There are  $\alpha(\text{Al})$  phases and coarse silicon phases in the matrix alloy, as shown in Fig. 7(a). Some black phases in the structure are added GNPs, as shown in Figs. 7(b)–(e). As can be seen from Fig. 7(b), the coarse eutectic silicon phase in the ADC12–0.3GNPs composite has been refined to a certain degree and becomes a short rod shape. The black phase is distributed at grain boundaries, and the grain size is also refined. As can be seen from Fig. 7(c), the amount of captured black phase particles in the ADC12–0.6GNPs composite is increased, the size of the silicon phase has been further refined, and the grains become smaller and smaller. As can be seen from Fig. 7(d), the amount of the captured black phase in the ADC12–

0.9GNPs composite is further increased, the dispersion is more uniform. The size and morphology of the silicon phases are optimized to a greater degree, the grains are also the most round, and the average grain size is about 18.5  $\mu\text{m}$ . When the content of added GNPs is 1.2 wt.%, some GNPs are agglomerated in the structure, and the silicon phase is also partially coarsened. The fineness of the grain size is weakened, and the average size is about 23.8  $\mu\text{m}$ , as shown in Fig. 7(e).

### 3.2.3 Microstructures of ADC12–GNPs composites prepared under different ultrasound time

Figure 8 shows the microstructures of ADC12–0.9GNPs composites, which were prepared under the conditions of ultrasonic power of 2.8 kW,



**Fig. 7** Microstructures of matrix and ADC12–GNPs composite with different graphene additions: (a) 0 wt.%; (b) 0.3 wt.%; (c) 0.6 wt.%; (d) 0.9 wt.%; (e) 1.2 wt.%

ultrasonic frequency of 20 kHz, and different ultrasonic time (6, 12, 18 min). When the ultrasonic time is 6 min, the GNP phase in the structure is partially agglomerated, and the average grain size is about 21.4  $\mu\text{m}$ , as shown in Fig. 8(a). When the ultrasonic time is 12 min, the GNP is dispersed uniformly, and there is almost no agglomeration. The average grain size is about 17.7  $\mu\text{m}$ , as shown in Fig. 8(b). When the ultrasonic time is 18 min, the uniformity of GNP is weakened, and the agglomeration of some GNPs occurs. The average grain size is about 19.5  $\mu\text{m}$ , as shown in Fig. 8(c).

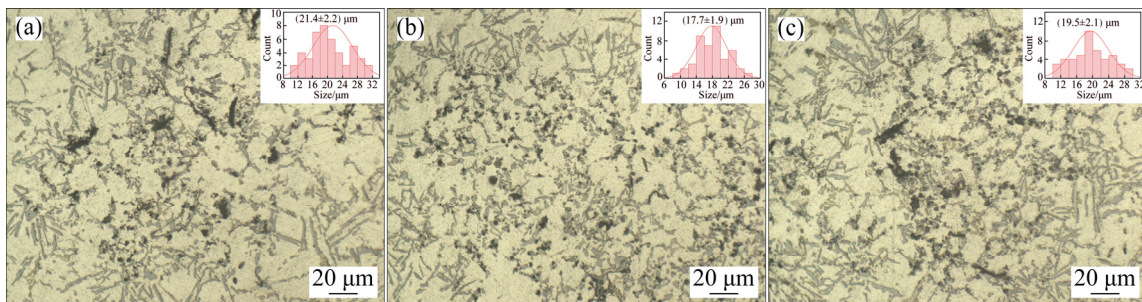
### 3.2.4 SEM analysis of ADC12–GNPs composite

Figure 9 shows the mapping results of different elements in ADC12–0.9GNPs composite prepared under high-intensity ultrasound conditions (the ultrasonic power of 2.8 kW, the ultrasonic frequency of 20 kHz, and the ultrasonic time of 12 min). The distribution of Al, Si, C, Cu, and Fe can be seen from Fig. 9. It can be seen that GNP

is sheet-shaped and distributed at a parallel, perpendicular or an angle with the matrix from Figs. 9(a) and (d). It can be seen that Al element is distributed in regions other than the C and Si elements from Fig. 9(b). It can be seen that the Si element is mainly distributed in the vicinity of GNP from Figs. 9(c) and (d). The distributions of Cu and Fe elements have nothing to do with distribution states of GNPs, both of them are more uniformly distributed throughout the SEM photograph, as shown in Figs. 9(e) and (f).

### 3.3 TEM analysis of composite

In order to study the state of the GNPs in the composite and its interface with the matrix, the composite was observed with a transmission electron microscope. Figure 10 shows the TEM analysis of ADC12–0.9GNPs composite prepared under the high-intensity ultrasound. A phase with the shape similar to GNP can be seen from



**Fig. 8** Microstructures of ADC12–0.9GNPs composites prepared under different ultrasound time: (a) 6 min; (b) 12 min; (c) 18 min

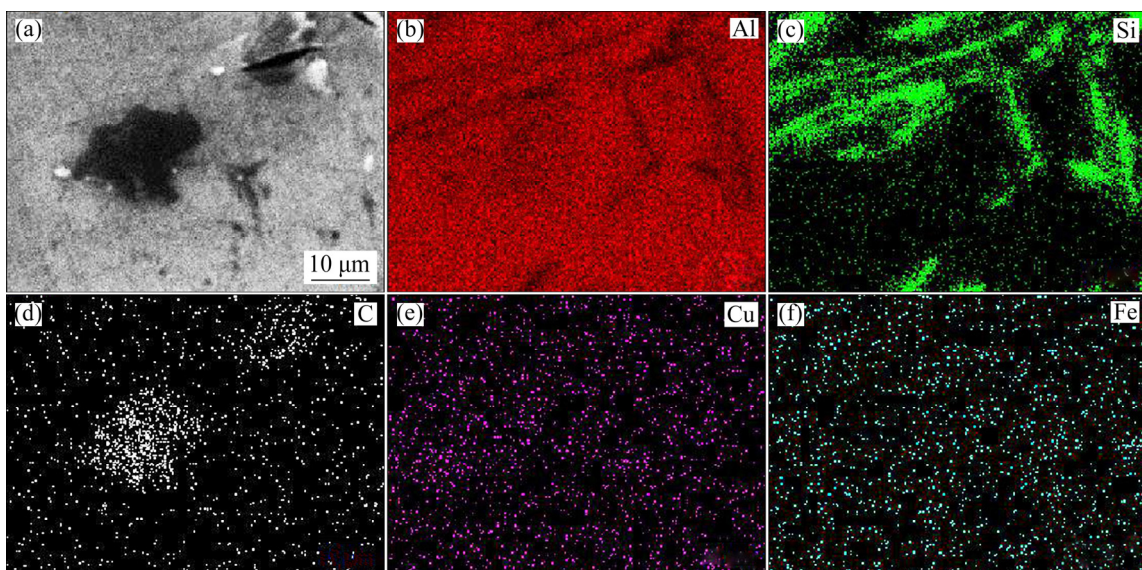


**Fig. 9** SEM image (a) and corresponding element distribution (b–f) of ADC12–0.9GNPs composite fabricated via high-intensity ultrasonic processing for 12 min

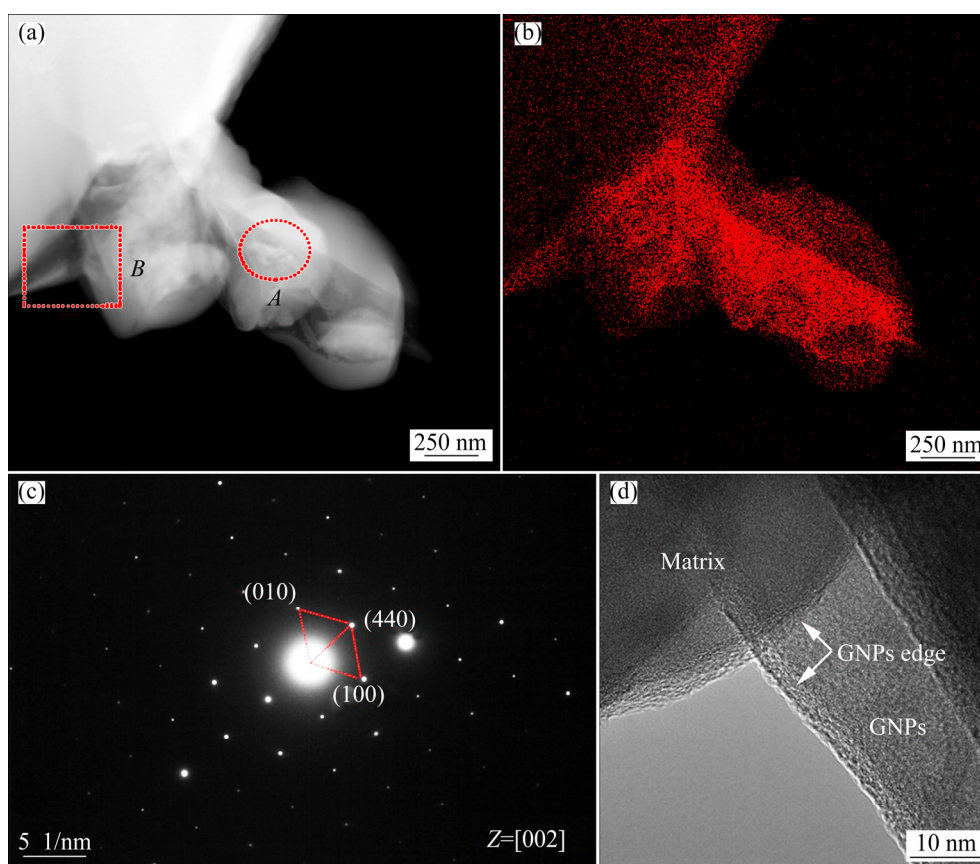


**Fig. 10** TEM images of ADC12–0.9GNPs composite: (a) High-angle annular dark-field image; (b) Mapping of C element; (c) SAED pattern of Region *A*; (d) Interface structure of Region *B*

Fig. 10(a). In order to determine the composition of the phase, the mapping result of C element in this region is shown in Fig. 10(b). The result shows that C element is concentrated. Therefore, it can be determined that materials with lamellar fold-like morphology are the added GNPs. Figure 10(c) shows the diffraction spot corresponding to Area *A* in Fig. 10(a). It can be seen that there are obvious boundary lines in the GNPs sheet region from Fig. 10(a), resulting from the slip and shift in one direction of GNPs. As a result, GNPs are opened under high-intensity ultrasound. It makes the sheet thinner, thus increasing the interfaces between GNPs and the matrix. For obtaining the interface structure information of GNPs and the matrix alloy, high resolution transmission electron microscopy (HRTEM) morphology observation was performed on Area *B* in Fig. 10(a), and the result is shown in Fig. 10(d). It can be seen that the interface between graphene and the substrate is very clean and tidy from Fig. 10(d). There are no long and brittle  $\text{Al}_4\text{C}_3$  phases nearby the interface, no holes and defects such as cracks, indicating that the interface

combination is good.

### 3.4 Mechanical properties

#### 3.4.1 Effect of GNPs content on mechanical properties of ADC12–GNPs composites.

Figure 11(a) shows the mechanical properties of the composite with different GNPs additions under the same ultrasonic conditions. It can be seen that the tensile strength and yield strength of the ADC12 alloy are 196 and 147.6 MPa, respectively, and the elongation is 2.39%. The mechanical properties of the materials are significantly improved after adding GNPs. When the addition of GNPs is 0.9 wt.%, the performance of the composite is better. At this time, the tensile strength and yield strength reach 256.8 and 210.6 MPa, respectively, and the elongation is 2.6 %, which are 30.5%, 42.7% and 8.4% higher than those of the matrix alloy, respectively. However, when the content of GNPs increases to 1.2 wt.%, the tensile strength and yield strength of the composite decrease to 241.5 and 193.2 MPa, respectively, which are still 22.7% and 30.9% higher than those

of the matrix alloy prepared under the same conditions. Figure 11(b) shows the microhardness of the material reinforced with different GNPs additions. It can be found that the hardness changing of the composite is to increase firstly, and then decreases. A higher value of HV 126.0 is gotten in ADC12–0.9 GNPs, which is 34.8% higher than that of the matrix alloy. When the content of GNPs is increased to 1.2 wt.%, the hardness of the composite decreases slightly to HV 114.4.

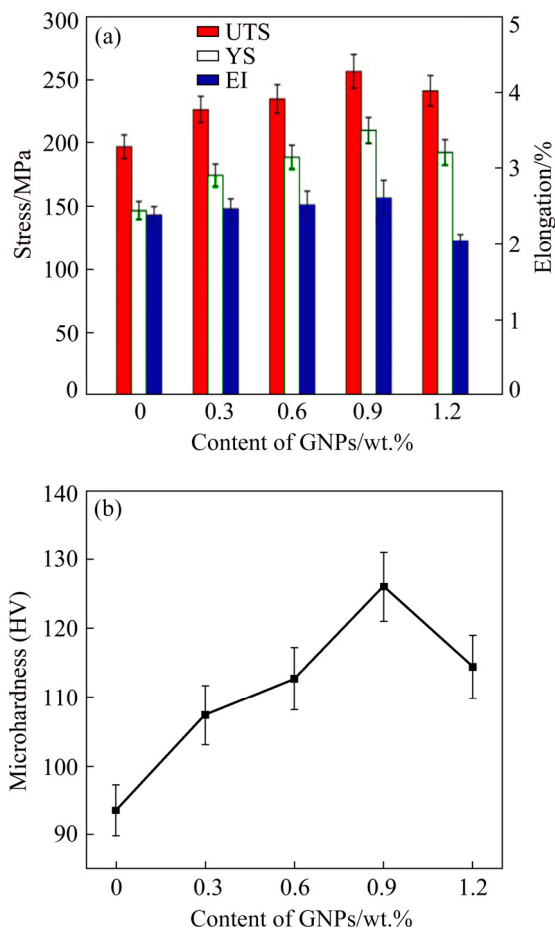


**Fig. 11** Effect of GNPs content on mechanical properties of ADC12–GNPs composites fabricated via high-intensity ultrasonic processing for 12 min: (a) Tensile properties; (b) Microhardness

### 3.4.2 Effect of ultrasonic time on mechanical properties of ADC12–GNPs composites

Figure 12(a) shows the tensile strength, yield strength and elongation of the ADC12–0.9 GNPs composite under different ultrasonic time. Under the same GNPs addition, the improvement of the tensile properties increases firstly, and then decreases with increasing the ultrasonic time. When the ultrasonic time is 6 min, the tensile strength and yield strength of the composite reach 244.2 and

195.1 MPa, respectively, and the elongation is 2.12%. When the ultrasonic time is 18 min, the tensile strength and yield strength of the composite reach 250.3 and 198.2 MPa, respectively, and the elongation is 2.28%. When the ultrasonic time is 12 min, the mechanical properties of the composite are better. The ultrasonic time has a similar effect on the hardness, as shown in Fig. 12(b).

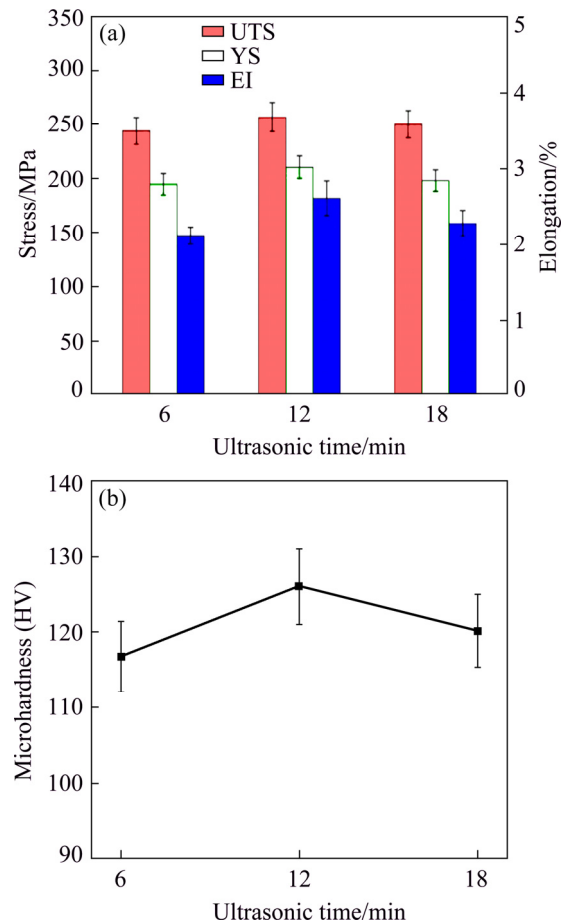


**Fig. 12** Effect of ultrasonic time on mechanical properties of ADC12–0.9GNPs composites: (a) Tensile properties; (b) Microhardness

### 3.5 Fracture analysis

Figures 13(a)–(c) show the fracture morphologies of the materials reinforced with different GNPs additions. It can be seen in Fig. 13(a) that the fracture morphology of the ADC12 alloy is mainly composed of cleavage fracture steps, tearing edges, coarse pores and longer cracks, showing an obvious brittle fracture. The coarse phases become the source of crack growth easily. After adding the GNPs, the fracture mechanism turns from a brittle fracture to a ductile fracture gradually, as shown in Figs. 13(b) and (c). When the amount of added GNPs is 0.9 wt.%, there

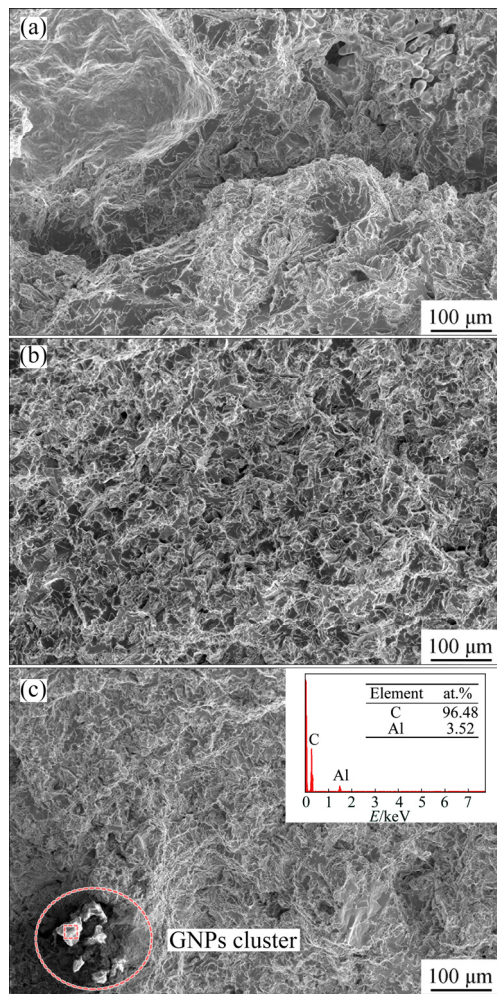


**Fig. 13** Fracture images of ADC12–GNPs composites treated under ultrasonic time of 12 min: (a) ADC12; (b) ADC12–0.9GNPs; (c) ADC12–1.2GNPs

are more dimples in the fracture of the composite, the distribution is more uniform, and the tearing edges become finer and more uniform, showing an obvious ductile fracture. When the amount of added GNPs is 1.2 wt.%, there are some aggregates with bright flaky morphology existing on the fracture. The energy spectrum analysis of the aggregates shows that the content of element C is high, indicating that the aggregates are GNPs, as shown in Fig. 13(c).

Figure 14 shows the high magnification scanning electron microscope fracture image of ADC12–1.2GNPs composite. It can be seen from the mapping analyses of the element C in Fig. 14(c) that the enriched area of the element C corresponds to the material with wrinkled sheet-like morphology in Fig. 14(a). In order to determine the composition of the substance more directly, four points were

selected for energy spectrum analysis. The corresponding point spectrum analysis results are shown in Figs. 14(f)–(i). It can be proved that these carbon elements enriched in the surface scan are all added GNPs, and the agglomeration of GNPs exists on the fracture structure of the composite.

### 3.6 Strengthening mechanism of ADC12–GNPs composite

#### 3.6.1 Impact of ultrasound

The Al–GNPs intermediate preforms release GNPs after being added to the melt. Due to the large specific surface area of GNPs, the surface energy is high, and it is easy to agglomerate. There are micro-bubbles inside the agglomerated GNPs, and the bonding force among the melts is weak in these places, becoming the nucleation core of cavitation bubbles. When the released huge energy acts on the melt, there will be acoustic cavitation and acoustic flow effects [29,30]. The instantaneous impact force generated by acoustic cavitation can overcome the van der Waals force among GNPs, and make the agglomerated GNPs dispersed. In addition, under the action of sound flow, the dispersed GNPs can be distributed more uniformly throughout the melt. Due to the excellent thermal conductivity of GNPs, during the solidification process, the effectively dispersed GNPs can make the heat of the silicon phase to the dendrites faster, thereby speeding up the cooling of the silicon phase and resulting in the refinement of the silicon phase. Besides, the silicon phase is mainly concentrated nearby GNPs, which also helps to suppress the harmful reaction between graphene and Al, and most GNPs have been preserved.

It can be found that when the melt temperature exceeds 2728 K (2455 °C), the thermodynamic Gibbs free energy ( $\Delta G$ ) of the reaction between Al and C is positive, and no reaction will occur to generate  $Al_4C_3$  [31]. The instantaneous high-temperature generated by the ultrasonic in the melt can reach  $10^4$  K, which can suppress the formation of brittle phase of  $Al_4C_3$  and avoid the structural damage of GNPs. At the same time, the local high-temperature of the melt can reduce the surface tension of GNPs and improve the wettability of Al melt and GNPs [32]. When the content of GNPs increases to a certain degree, the agglomeration of GNPs and the viscosity of the melt increase under the same ultrasonic power. Moreover, the ultrasonic

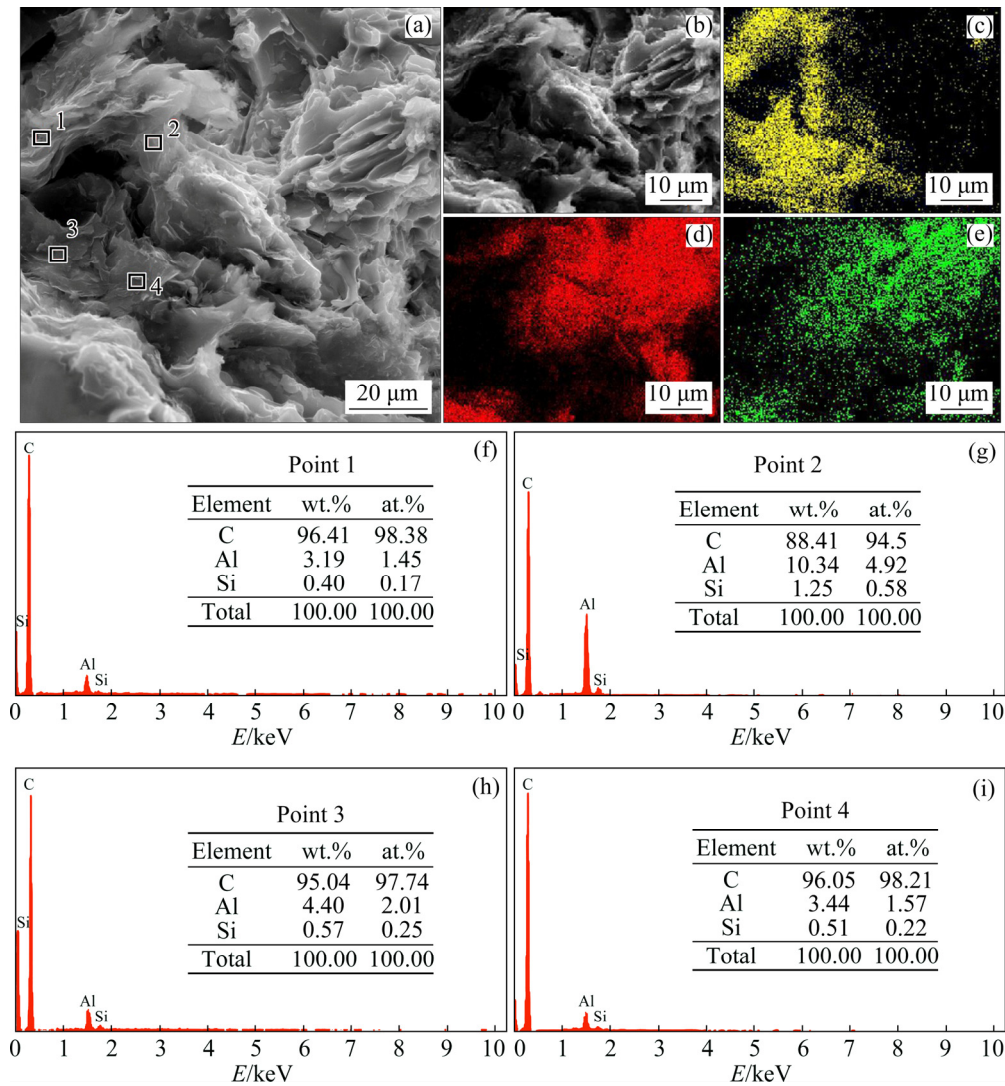


**Fig. 14** SEM fracture images and corresponding EDS results of ADC12–1.2GNPs composites: (a) High magnification fracture image; (b) Mapping analysis of Fig.(a); (c) Mapping image of C; (d) Mapping image of Al; (e) Mapping image of Si; (f) EDS of Point 1; (g) EDS of Point 2; (h) EDS of Point 3; (i) EDS of Point 4

dispersion ability is limited, and it is not enough to make it dispersed completely, causing partial aggregation. When the addition of GNPs and the other ultrasound conditions are the same, the released shock waves by the short time ultrasound can not disperse the aggregated GNPs, leading to the agglomeration of some GNPs. If the ultrasound time is too long, continuous ultrasonic vibration will cause frequent collisions among GNPs, which will make GNPs re-aggregate. Therefore, choosing the appropriate ultrasonic process parameters and the addition of GNPs can disperse GNPs in the matrix effectively, and also help to obtain a good interface.

### 3.6.2 Fine grain strengthening

After adding GNPs to the melt, the grain size has been changed greatly. The reason is that the

high-intensity ultrasound allows GNPs to be dispersed in the melt. The dispersed GNPs form a large area grid structure along the grain boundaries, which suppresses the diffusion and growth of the grains. The more uniform the GNPs are, the finer the grains are. Meanwhile, the grain boundaries are denser and denser, and the higher the energy consumed by the crack propagation and diffusion generated by the external force. It is more difficult for cracks to propagate, so the fine grain strengthening effect brought by GNPs is more obvious. The strength increased by this factor can be calculated by the Hall–Petch formula [33]:

$$\Delta\sigma_{\text{Hall-Petch}} = k(d_{\text{com}}^{-1/2} - d_{\text{alloy}}^{-1/2}) \quad (1)$$

where  $d_{\text{com}}$  and  $d_{\text{alloy}}$  are the average grain sizes of the composite material and the matrix alloy,

respectively;  $k$  is the Hall–Petch coefficient for aluminum alloys ( $68 \text{ MPa} \cdot \mu\text{m}^{1/2}$ ) and  $\Delta\sigma_{\text{Hall-Petch}}$  is the corresponding increase in yield strength for grain refinement of composite materials. As the addition of graphene refines the grains of the matrix alloy, the smaller the grain size, the larger the value of  $d_{\text{com}}^{-1/2}$ , so the value of  $\Delta\sigma_{\text{Hall-Petch}}$  increases, and finally the strength of the composite material is enhanced.

### 3.6.3 Dislocation strengthening due to difference in thermal expansion coefficients

The thermal expansion coefficient of pure aluminum is  $2.36 \times 10^{-5} \text{ K}^{-1}$ , while the thermal expansion coefficient of graphene is  $-1 \times 10^{-6} \text{ K}^{-1}$ . Therefore, the great difference in thermal expansion coefficient between aluminum matrix and graphene makes a large number of dislocations to be formed to strengthen the effect. Figure 15 shows the TEM image of dislocations in the ADC12–GNPs composite.

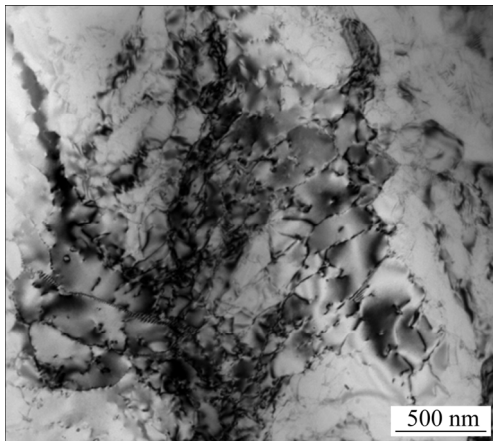


**Fig. 15** TEM image of dislocation in ADC12–GNPs composite

The strength increased by this factor can be calculated by the Hall–Petch formula [34]:

$$\Delta\sigma_{\text{CET}} = \alpha G b \sqrt{\frac{12\Delta T \Delta C f_v}{b d_p}} \quad (2)$$

where  $G$  is the shear modulus of aluminum ( $2.7 \times 10^{10} \text{ N/m}^2$ ),  $b$  is the Berkeley vector component of the aluminum matrix ( $2.84 \times 10^{-10} \text{ m}$ ),  $\alpha$  is a constant (the value is 1.25),  $\Delta T$  is the temperature change,  $\Delta C$  is the difference of the thermal expansion coefficients between GNPs and aluminum matrix,  $f_v$  is the volume fraction of GNPs,  $d_p$  is the average size of GNPs, and  $\Delta\sigma_{\text{CET}}$  is the yield strength increase of the composite.

### 3.6.4 Load transfer enhancement

Load transfer strengthening also illustrates the reinforcing effect of GNPs. Loads are transferred from the matrix to the graphene reinforcing phase through interface shear stress, which makes full use of the excellent mechanical properties of GNPs. The higher the interface bonding strength of ADC12–GNPs, the more obvious the load transfer enhancement effect. The incremental expression of the mechanism's contribution to the yield strength of composites ( $\Delta\sigma_{\text{LT}}$ ) can be calculated using the following formula [35]:

$$\Delta\sigma_{\text{LT}} = \frac{f_v \sigma_m}{2} \quad (3)$$

where  $\sigma_m$  is the yield strength of the aluminum matrix.

### 3.6.5 Calculation of strengthening values

Using the above theoretical model, the contribution of each strengthening mechanism to the yield strength of the composite can be calculated. The results are shown in Fig. 16(a). By superimposing each strengthening mechanism, the theoretical prediction model of yield strength of ADC12–GNPs composite can be obtained.

$$\sigma_{\text{Theoretic}} = \sigma_m + \Delta\sigma_{\text{Hall-Petch}} + \Delta\sigma_{\text{CET}} + \Delta\sigma_{\text{LT}} \quad (4)$$

The formula (4) is used to predict the theoretical yield strength of the composite. It can be seen from Fig. 16(a) that the yield strength contributed by the fine grain strengthening mechanism is low, and the yield strength contributed by the dislocation strengthening or load transfer strengthening mechanism is high. As can be seen from Fig. 16(b), the values of theoretical yield strength are higher than those of experimental yield strength. Moreover, the discrepancy of yield strength between the two curves increases with an increase of the amount of GNPs. The discrepancy of the detrimental variation trend may be attributed to the agglomeration of GNPs cluster, resulting in the weak bonding strength between the GNPs and the matrix. In addition, the uneven layers or the inconsistent orientation of GNPs on the substrate is also the reason why the experimental value differs from the theoretical value greatly.

### 3.6.6 Strengthening model diagram

In order to understand the mechanism that GNPs enhanced ADC12 aluminum matrix composites easily under the action of high-intensity ultrasound, Fig. 17 shows the schematic diagrams

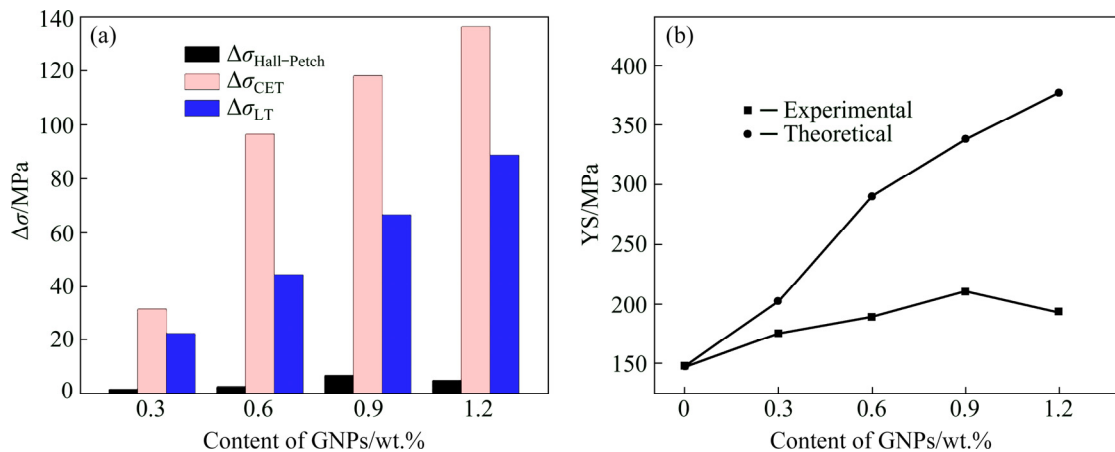


**Fig. 16** Increment of yield strength contributed by different strengthening mechanisms (a) and comparison of theoretical and experimental yield strengths (b)

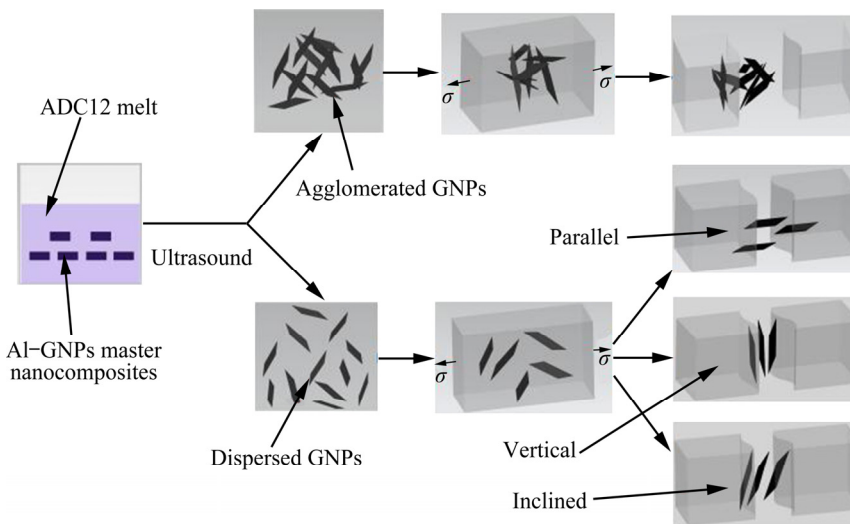


**Fig. 17** Sketch diagrams of strengthening model of ADC12–GNPs composite

of strengthening model of the composite. The added GNPs can be scattered by the impact of the ultrasound. When the ultrasonic time is too short or too long, or the amount of added GNPs is excessive, GNPs will agglomerate in the matrix, and holes and micro-crack defects will breed and expand among the agglomerated GNPs easily. The strengthening effect becomes worse. In addition, the agglomerated GNPs can cause the easy sliding between the GNP–GNP and Al–GNP–Al grains due to solid lubricant property of GNPs. Therefore, as the graphene aggregates, its role will change from a reinforcing element to a solid lubricating material gradually, which has a negative effect on the mechanical behavior of composites.

When the appropriate amount of GNPs is added and the appropriate ultrasonic time is

applied, GNPs will be dispersed in the melt effectively. There are three distribution states of the dispersed few layers of GNPs in the matrix: the first situation is parallel to the direction of the tensile sample, the second situation is vertical to the direction of the tensile sample, and the third situation is inclined to the direction of the tensile sample. The GNPs in the first distributed state can absorb more loads transferred from the matrix and make the most contribution to the mechanical properties of the composite. The GNPs in the second distribution state absorb less load transferred from the substrate, overcoming mainly the binding energy. The contribution of GNPs in the third distribution state to the mechanical properties of composites is between the two states.

## 4 Conclusions

(1) Metal matrix composites based on aluminum alloy ADC12 reinforced with graphene nanoplates were fabricated by high-intensity ultrasonic assisted casting.

(2) Liquid dispersion can promote the uniform mixing between the aluminum powder and GNPs, and the structural integrity of GNPs was preserved. High-intensity ultrasound can promote the uniform distribution of GNPs in the melt, resulting in refining the  $\alpha(\text{Al})$  phase and the Si phase.

(3) The effects of different graphene additions (0.3, 0.6, 0.9, 1.2 wt.%) and ultrasonic time (6, 12, 18 min) on the microstructure and mechanical properties were reported. Under the same ultrasonic conditions, the refinement of the microstructure increased firstly, and then decreased with increasing the content of GNPs. The ultrasonic time had the similar effect on the refinement of the microstructure. When the ultrasonic power was 2.8 kW, the ultrasonic frequency was 20 kHz, the ultrasonic temperature was 780 °C, the optimal GNPs content was 0.9 wt.%, and the optimal ultrasonic time was 12 min. The tensile strength, the yield strength and the hardness of the composite produced under the optimal ultrasonic parameters were 256.8 MPa, 210.6 MPa and HV 126.0, respectively, which increased by 30.5%, 42.7% and 34.8% compared with those of the matrix alloy, respectively.

(4) The change trends of the mechanical properties were consistent with the microstructures of ADC12–GNPs composites. After adding the GNPs, the fracture mechanism gradually turned from a brittle fracture to a ductile fracture. In addition, high-intensity ultrasound can inhibit the formation of the  $\text{Al}_4\text{C}_3$  brittle phase. The good interface and distribution allowed GNPs to play the role in fine grain strengthening, dislocation strengthening and load transfer strengthening effectively, improving the comprehensive mechanical properties of the composites remarkably.

## References

[1] ZOU Xiu-liang, YAN Hong, CHEN Xiao-hui. Evolution of second phases and mechanical properties of 7075 Al alloy

- processed by solution heat treatment [J]. Transactions of Nonferrous Metals Society of China, 2017, 27: 2146–2155.
- [2] MONIKANDAN V V, RAJENDRAKUMAR P K, JOSEPH M A. High temperature tribological behaviors of aluminum matrix composites reinforced with solid lubricant particles [J]. Transactions of Nonferrous Metals Society of China, 2020, 30: 1195–1210.
- [3] WU Qing-jie, YAN Hong, ZHANG Peng-xiang, ZHU Xue-qin, NIE Qiao. Enhancing wear resistance of A356 alloy by adding CNFs based on ultrasonic vibration casting [J]. Acta Metallurgica Sinica (English Letters), 2018, 31: 523–532.
- [4] DAVID RAJA SELVAM J, DINAHARAN I, VIBIN PHILIP S, MASHININI P M. Microstructure and mechanical characterization of in situ synthesized AA6061/(TiB<sub>2</sub>+Al<sub>2</sub>O<sub>3</sub>) hybrid aluminum matrix composites [J]. Journal of Alloys and Compounds, 2018, 740: 529–535.
- [5] KUILA T, BOSE S, MISHRA A K, KHANRA P, KIM N H, LEE J H. Chemical functionalization of graphene and its applications [J]. Progress in Materials Science, 2012; 57: 1061–1105.
- [6] WANG Jian, GUO Li-na, LIN Wan-ming, CHEN Jin, ZHANG Shuai, CHEN Shao-da, ZHEN Tian-tian, ZHANG Yu-yang. The effects of graphene content on the corrosion resistance, and electrical, thermal and mechanical properties of graphene/copper composites [J]. New Carbon Materials, 2019, 34(2): 161–169.
- [7] SUN Ling. Structure and synthesis of graphene oxide [J]. Chinese Journal of Chemical Engineering, 2019, 27: 2251–2260.
- [8] GAO Xin, YUE Hong-yan, GUO Er-jun, ZHANG Shao-lin, WANG Bao, GUAN En-hao, SONG Shan-shan, ZHANG Hong-jie. Preparation and tribological properties of homogeneously dispersed graphene-reinforced aluminium matrix composites [J]. Materials Science and Technology, 2018, 34(11): 1316–1322.
- [9] BASTWROS M, KIM G Y, ZHU Can, ZHANG Kun, WANG Shi-ren, TANG Xiao-duan, WANG Xin-wei. Effect of ball milling on graphene reinforced Al6061 composite fabricated by semi-solid sintering [J]. Composites: Part B, 2014, 60: 111–118.
- [10] SENEL M C, GURBUZ M, KOC E. Fabrication and characterization of aluminum hybrid composites reinforced with silicon nitride/graphene nanoplatelet binary particles [J]. Journal of Composite Materials, 2019, 53(28–30): 4043–4054.
- [11] LIU Guang, ZHAO Nai-qin, SHI Chun-sheng, LIU En-zuo, HE Fang, MA Li-ying, LI Qun-ying, LI Jia-jun, HE Chun-nian. In-situ synthesis of graphene decorated with nickel nanoparticles for fabricating reinforced 6061Al matrix composites [J]. Materials Science & Engineering A, 2017, 699: 185–193.
- [12] BHADARIA A, SINGH L K, LAHA T. Effect of physio-chemically functionalized graphene nanoplatelet reinforcement on tensile properties of aluminum nanocomposite synthesized via spark plasma sintering [J]. Journal of Alloys and Compounds, 2018, 748: 783–793.
- [13] LI Min, GAO Hai-yan, LIANG Jia-miao, GU Sun-wang, YOU We-ren, SHU Da, WANG Jun, SUN Bao-de.

- Microstructure evolution and properties of graphene nanoplatelets reinforced aluminum matrix composites [J]. *Materials Characterization*, 2018, 140: 172–178.
- [14] ZENG Xiang, TENG Jie, YU Jin-gang, TAN Ao-shuang, FU Ding-fa, ZHANG Hui. Fabrication of homogeneously dispersed graphene/Al composites by solution mixing and powder metallurgy [J]. *International Journal of Minerals, Metallurgy and Materials*, 2018, 25(1): 102–109.
- [15] AKBARPOUR M R, POURESMAEIL A. The influence of CNTs on the microstructure and strength of Al-CNT composites produced by flake powder metallurgy and hot pressing method [J]. *Diamond & Related Materials*, 2018, 88: 6–11.
- [16] XU Wei, LU Xin, HAYAT M D, TIAN Jing-jing, HUANG chao, CHEN Miao, QU Xuan-hui, WEN Cui-e. Fabrication and properties of newly developed Ti35Zr28Nb scaffolds fabricated by powder metallurgy for bone-tissue engineering [J]. *Journal of Materials Research and Technology*, 2019, 8(5): 3696–3704.
- [17] ABBASIPOUR B, NIROUMAND B, MONIR VAGHEFI S M, ABEDI M. Tribological behavior of A356-CNT nanocomposites fabricated by various casting techniques [J]. *Transactions of Nonferrous Metals Society of China*, 2019, 29: 1993–2004.
- [18] RAMANATHAN A, PRADEEP K K, RAJARAMAN M. A review on the production of metal matrix composites through stir casting-Furnace design, properties, challenges, and research opportunities [J]. *Journal of Manufacturing Processes*, 2019, 42: 213–245.
- [19] AYDIN O, KOCAVELI A, GURSOY O, ERZI E, DISPINAR D. Aluminum matrix graphene-reinforced composite materials [J]. *The Minerals, Metals & Materials Society*, 2019: 365–371. <https://doi.org/10.1007/978-3-030-06034-3>.
- [20] VENKATESAN S, XAVIOR M A. Tensile behavior of aluminum alloy (AA7050) metal matrix composite reinforced with graphene fabricated by stir and squeeze cast processes [J]. *Science and Technology of Materials*, 2018, <https://doi.org/10.1016/j.stmat.2018.02.005>.
- [21] LIU Shi-ying, GAO Fei-peng, ZHANG Qiong-yuan, ZHU Xue, LI Wen-zhen. Fabrication of carbon nanotubes reinforced AZ91D composites by ultrasonic processing [J]. *Transactions of Nonferrous Metals Society of China*, 2010, 20: 1222–1227.
- [22] YUAN Du, YANG Xiong, WU Shu-sen, LÜ Shu-lin, HU Kun. Development of high strength and toughness nano-SiC<sub>p</sub>/A356 composites with ultrasonic vibration and squeeze casting [J]. *Journal of Manufacturing Processes*, 2019, 269: 1–9.
- [23] HU Zhi, YAN Hong, RAO Yuan-sheng. Effects of samarium addition on microstructure and mechanical properties of as-cast Al–Si–Cu alloy [J]. *Transactions of Nonferrous Metals Society of China*, 2013, 23: 3228–3234.
- [24] FARAHANY S, OURDJINI A, BAKAR T A A, IDRIS M H. A new approach to assess the effects of Sr and Bi interaction in ADC12 Al–Si die casting alloy [J]. *Thermochimica Acta*, 2014, 575: 179–187.
- [25] OKAYASU M, OHKURA Y, TAKEUCHI S, TAKASU S, OHFUJI H, SHIRAISHI T. A study of the mechanical properties of an Al–Si–Cu alloy (ADC12) produced by various casting processes [J]. *Materials Science and Engineering A*, 2012, 543: 185–192.
- [26] RASHAD M, PAN Fu-sheng, ASIF M, TANG Ai-tao. Powder metallurgy of Mg–1%Al–1%Sn alloy reinforced with low content of graphene nanoplatelets (GNPs) [J]. *Journal of Industrial and Engineering Chemistry*, 2014, 20: 4250–4255.
- [27] DUN Yu-chao, ZUO Yu. Preparation and characterization of a GPTMS/graphene coating on AA-2024 alloy [J]. *Applied Surface Science*, 2017, 416: 492–502.
- [28] KUMAR H G P, PRABHAKARAN S, XAVIOR M A, KALAINATHAN S, LIN Dong, SHUKLA P, VASUDEVAN V K. Enhanced surface and mechanical properties of bioinspired nanolaminate graphene-aluminum alloy nanocomposites through laser shock processing for engineering applications [J]. *Materials Today Communications*, 2018, 16: 81–89.
- [29] CHEN Xiao-hui, YAN Hong. Fabrication of nanosized Al<sub>2</sub>O<sub>3</sub> reinforced aluminum matrix composites by subtype multifrequency ultrasonic vibration [J]. *Journal of Materials Research*, 2015, 30(14): 2197–2208.
- [30] SAUTER C, EMIN M A, SCHUCHMANN H P, TAVMAN S. Influence of hydrostatic pressure and sound amplitude on the ultrasound induced dispersion and de-agglomeration of nanoparticles [J]. *Ultrasonics Sonochemistry*, 2008, 15: 517–523.
- [31] CI L, RYU Z, JIN-PHILLIPP N Y, RUHLE M. Investigation of the interfacial reaction between multi-walled carbon nanotubes and aluminum [J]. *Acta Materials*, 2006, 54(20): 5367–5375.
- [32] GALLEGUILLOS-SILVA R, VARGAS-HERNÁNDEZ Y, GAETE-GARRETÓN L. Wettability of a surface subjected to high frequency mechanical vibrations [J]. *Ultrasonics Sonochemistry*, 2017, (35): 134–141.
- [33] WYRZYKOWSKI J W, GRABSKI M W. The Hall–Petch relation in aluminium and its dependence on the grain boundary structure [J]. *Philosophical Magazine A*, 1986, 53(4): 505–520.
- [34] LUSTER J W, THUMANN M, BAUMANN R. Mechanical properties of aluminium alloy 6061-Al<sub>2</sub>O<sub>3</sub> composites [J]. *Journal of Industrial and Engineering Chemistry*, 1993, 9(10): 853–862.
- [35] RASHAD M, PAN Fu-sheng, TANG Ai-tao, ASIF M, HUSSAIN S, GOU Jun, MAO Jian-jun. Improved strength and ductility of magnesium with addition of aluminum and graphene nanoplatelets (Al + GNPs) using semi powder metallurgy method [J]. *Journal of Industrial and Engineering Chemistry*, 2015, 23: 243–250.

# 超声熔铸法制备石墨烯纳米片增强 ADC12 复合材料的显微组织及力学性能

熊俊杰<sup>1,2</sup>, 闫洪<sup>1,2</sup>

1. 南昌大学 机电工程学院, 南昌 330031;

2. 南昌市轻合金材料制备与加工重点实验室, 南昌 330031

**摘要:** 采用高能超声熔铸法制备石墨烯纳米片增强 ADC12 铝基复合材料, 并对其显微组织及力学性能进行研究。实验结果表明, 高能超声可有效促进石墨烯纳米片在熔体中的均匀分散, 同时石墨烯纳米片的加入能细化  $\alpha(\text{Al})$  相和 Si 相。得到较优的石墨烯纳米片添加量是 0.9%(质量分数), 较优的超声时间是 12 min, 在该参数下制备的复合材料抗拉强度、屈服强度和显微硬度分别为 256.8 MPa、210.6 MPa 和 HV 126.0, 与相同条件下的基体合金相比分别提高 30.5%、42.7%和 34.8%。基体中加入石墨烯纳米片后, 其断裂机制逐步由脆性断裂向韧性断裂转变。良好界面的结合和分散性的改善使得复合在基体中的石墨烯纳米片能更好地发挥细晶强化、位错强化和载荷转移强化作用。

**关键词:** ADC12 复合材料; 石墨烯纳米片(GNP); 熔铸; 组织; 力学性能

(Edited by Xiang-qun LI)